energies

MDPI

Article

Solar Hydrogen Production via a Samarium Oxide-Based Thermochemical Water Splitting Cycle

Rahul Bhosale [1,*], Anand Kumar [1], Fares AlMomani [1], Ujjal Ghosh [1], Mohammad Saad Anis [1], Konstantinos Kakosimos [2], Rajesh Shende [3] and Marc A. Rosen [4]

1 Department of Chemical Engineering, College of Engineering, Qatar University, P. O. Box 2713, Doha 2713, Qatar; akumar@qu.edu.qa (A.K.); falmomani@qu.edu.qa (F.A.); ughosh@qu.edu.qa (U.G.); ma1304725@student.qu.edu.qa (M.S.A.)

2 Department of Chemical Engineering, Texas A&M University at Qatar, PO Box 23874, Doha 2713, Qatar; k.kakosimos@qatar.tamu.edu

3 Department of Chemical and Biological Engineering, South Dakota School of Mines and Technology, Rapid City, SD 57701-3995, USA; rajesh.Shende@sdsmt.edu

4 Faculty of Engineering and Applied Science, University of Ontario Institute of Technology, 2000 Simcoe St. North, Oshawa, ON L1H 7K4, Canada; Marc.Rosen@uoit.ca

* Correspondence: rahul.bhosale@qu.edu.qa; Tel.: +974-4403-4168

Academic Editor: Wei-Hsin Chen

Received: 25 January 2016; Accepted: 18 April 2016; Published: 25 April 2016

Abstract: The computational thermodynamic analysis of a samarium oxide-based two-step solar thermochemical water splitting cycle is reported. The analysis is performed using HSC chemistry software and databases. The first (solar-based) step drives the thermal reduction of Sm_2O_3 into Sm and O_2. The second (non-solar) step corresponds to the production of H_2 via a water splitting reaction and the oxidation of Sm to Sm_2O_3. The equilibrium thermodynamic compositions related to the thermal reduction and water splitting steps are determined. The effect of oxygen partial pressure in the inert flushing gas on the thermal reduction temperature (T_H) is examined. An analysis based on the second law of thermodynamics is performed to determine the cycle efficiency (η_{cycle}) and solar-to-fuel energy conversion efficiency ($\eta_{solar-to-fuel}$) attainable with and without heat recuperation. The results indicate that η_{cycle} and $\eta_{solar-to-fuel}$ both increase with decreasing T_H, due to the reduction in oxygen partial pressure in the inert flushing gas. Furthermore, the recuperation of heat for the operation of the cycle significantly improves the solar reactor efficiency. For instance, in the case where T_H = 2280 K, η_{cycle} = 24.4% and $\eta_{solar-to-fuel}$ = 29.5% (without heat recuperation), while η_{cycle} = 31.3% and $\eta_{solar-to-fuel}$ = 37.8% (with 40% heat recuperation).

Keywords: solar thermochemical; thermodynamics; hydrogen; water splitting; samarium oxide; computational analysis

1. Introduction

Two concerns in many countries are long-term shortages of fossil fuels and the need to secure fuel supplies. Carbon dioxide emissions constitute another significant issue concerning all societies, as such emissions are considered the main cause of global warming and climate change, for which the consequences are predicted to be melting of glaciers, a sea level rise, and increased weather extremes. The CO_2 emissions from fuel combustion were 32.1 Gt (billion metric tons) in 2015 [1]. As a consequence, it is important for countries to invest in and shift towards clean energy technologies such as solar energy.

The conversion of solar energy to chemical energy in the form of an alternative fuel such as H_2 provides a promising future sustainable energy pathway. Hydrogen can be produced with solar thermal energy via water splitting reactions. Hydrogen used in this manner is an energy carrier. Its advantages include a high energy density (on a mass basis) and non-polluting nature.

The metal oxide (MO)-based two-step solar thermochemical cycle is a potentially advantageous way to produce hydrogen via water splitting [2–4]. The main reactions involved in the MO based two-step solar thermochemical water splitting cycle are as follows:

Reaction 1: Solar thermal dissociation of MO:

$$MO \rightarrow MO_{reduced} + O_2 \quad (1)$$

Reaction 2: Non-solar water splitting step:

$$MO_{reduced} + H_2O \rightarrow MO + H_2 \quad (2)$$

The MO-based two-step solar thermochemical water splitting cycle is beneficial because it avoids the formation of an explosive gaseous mixture of H_2 and O_2 (since both gases are produced in different steps). Furthermore, the MO can be used in multiple thermochemical cycles as it is not consumed during any of the steps involved.

In the past, several MO-based redox systems were theoretically and experimentally studied as potential thermochemical water splitting reactions. These include zinc oxide cycles [2–11], iron oxide cycles [12–15], tin oxide cycles [16–18], terbium oxide cycles [19], mixed ferrite cycles [20–25], ceria cycles [26–29], and perovskite cycles [30–32]. In the case of zinc and tin oxide cycles, due to the volatile nature of the MOs involved, the loss of reactive material due to high temperature operation is inevitable. In the case of the iron oxide, ferrite, ceria, and perovskite cycles, the complete reduction of the MOs is not possible and hence a lower H_2 production is expected (per kg of metal oxide and per unit solar energy input). Therefore, investigations of new thermochemical cycles aimed at H_2 production via solar thermochemical water splitting are needed.

In this paper, the thermodynamic feasibility of a novel samarium oxide-based two-step solar thermochemical water splitting (Sm-WS) cycle is investigated. This is, to the best of the authors' knowledge, the first time that a Sm-WS cycle has been investigated for use in solar H_2 production. Thermodynamic modeling of the Sm-WS cycle is performed (in two sections) using the commercial thermodynamic HSC Chemistry software and databases [33]. In section one, the thermodynamic equilibrium compositions during the solar thermal reduction of Sm_2O_3 and the oxidation of Sm via water splitting are determined. The effect of the oxygen partial pressure in the inert flushing gas used inside a solar reactor during thermal reduction of Sm_2O_3 is examined. Also, the variation in the Gibbs free energy as a function of water splitting temperature (T_L) for the H_2 production step is estimated. In section two, energy and exergy analyses of the Sm-WS cycle are carried out. The solar reactor absorption efficiency, the required solar energy input, radiation heat losses, the rate of heat rejected by the quench unit and the water splitting reactor, and the solar-to-fuel conversion efficiency of the Sm-WS cycle are determined via computational thermodynamic modeling and the results are reported. A typical Sm-WS cycle is presented in Figure 1.

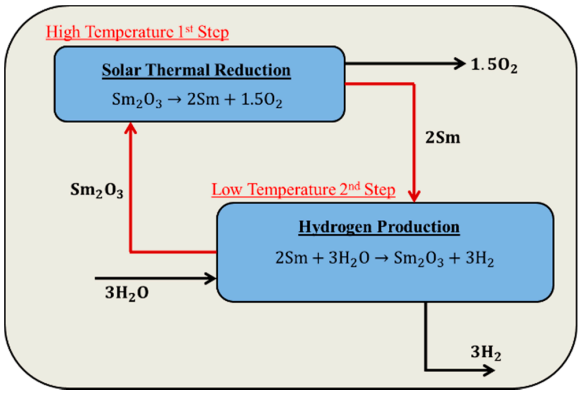

Figure 1. Typical Sm-WS cycle.

To perform the thermodynamic calculations in a conventional way, we rely on the experimental or assessed data (which utilizes stability functions) published in thermodynamic books and scientific journals. This approach is time consuming due to the difficulty in locating the thermodynamic data in the published literature and also because the calculations involved are complicated. Furthermore, inconsistencies arising from the use of different standard and reference states make the final results uncomparable. HSC Chemistry software and its databases permit rapid and straightforward conventional thermodynamic calculations on personal computers. The software provides calculation procedures for investigating the influence of different variables on a chemical system at equilibrium. In addition to the thermodynamic calculations, with the help of HSC Chemistry software and its databases, heat and material balance calculations for processes can be carried out straightforwardly, especially compared to manual methods. The dissolution and corrosion behavior of materials can also be studied in an expedite way using the Eh-pH-diagrams available in HSC Chemistry software. One of the limitations associated with the software is its inability to solve all chemical problems as it does not take into account the kinetics of chemical reactions. Nevertheless, it can be used to determine the optimal reaction conditions and yields of experiments (without carrying out actual expensive experiments) in an economical and effective manner. The name of the software is based on the fact that it performs calculations utilizing thermochemical database related to enthalpy (H), entropy (S), and heat capacity (Cp), for more than 28,000 chemical species. Due to these features, HSC has been widely used for a range of applications in academia, industry and research.

With an average concentration of about 8 parts per million (ppm), samarium is the 40th most abundant element in the Earth's crust. It is the fifth most abundant lanthanide and is more common than elements such as tin. Samarium oxides are readily available from commercial suppliers such as Sigma Aldrich. It can be synthesized inexpensively in laboratories using various synthesis approaches, such as combustion synthesis, the sol-gel method and the co-precipitation method, as samarium precursors such as samarium nitrate are available at a low cost. Samarium does not pose a threat to environment, including plants and animals. The melting points for Sm_2O_3 and Sm are 2608 and 1347 K, respectively. Similarly, the ΔH and ΔS values for the decomposition of Sm_2O_3 (according the reaction chemistry mentioned in Figure 1) are equal to 2240.5 kJ and 0.527 kJ/K, respectively.

2. Chemical Thermodynamic Equilibrium

The Sm-WS cycle mainly involves the following reactions:

$$Sm_2O_3 \rightarrow 2Sm + 1.5O_2\,(g) \quad (3)$$

$$2Sm + 3H_2O \rightarrow Sm_2O_3 + 3H_2\,(g) \quad (4)$$

According to the reaction chemistry, three moles of H_2 can be produced in one complete thermochemical cycle including one thermal reduction and one water splitting step. This seems to be an advantage of the Sm-WS cycle over previously investigated thermochemical cycles, as they are capable of producing either 1 or less than 1 mole of H_2 in one complete thermochemical cycle. To perform the energy and exergy analyses, thermodynamic data for all the reactive species involved (as shown in Equations (3) and (4)) are taken from HSC and the analyses are performed assuming continuous operation of the solar reactor with an inlet molar flow rate of Sm_2O_3 of 1 mol$\cdot$ s^{-1}.

As reported in previous studies [14,19,29], the temperature required for the thermal reduction of MOs can be reduced using an inert flushing gas such as ultra-high purity Ar with an oxygen partial pressure in the range of 10^{-5} to 10^{-8} bar. From this viewpoint, the effect of the oxygen partial pressure in the inert flushing gas on the thermal reduction of Sm_2O_3 is examined. According to Figure 2, as the oxygen partial pressure in the inert flushing gas is decreased, T_H can be significantly reduced. For instance, at oxygen partial pressure of 10^{-5} bar, the complete thermal reduction of Sm_2O_3 can be achieved at 3000 K. As the oxygen partial pressure is further lowered to 10^{-6}, 10^{-7}, and 10^{-8} bar, the required T_H values decease to 2780, 2540, and 2280 K, respectively.

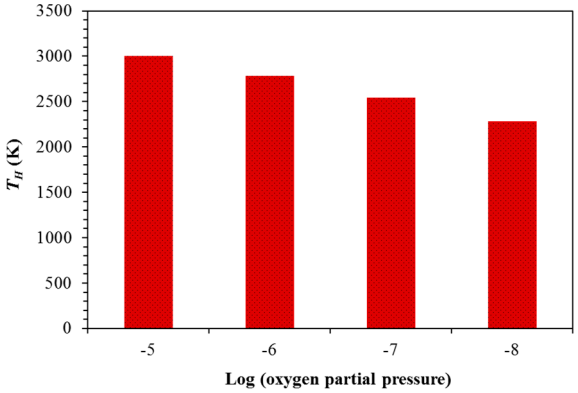

Figure 2. Effect of oxygen partial pressure in the inert flushing gas on T_H.

The influence of oxygen partial pressure in the inert flushing gas on the equilibrium compositions associated with the thermal reduction of Sm_2O_3 is also studied. As per the results in Figure 3a–c, the slope of the decrease in the molar concentration of Sm_2O_3 and the increase in the molar concentration of Sm(g) and O_2(g) both shift towards lower T_H with a reduction in the oxygen partial pressure in the inert flushing gas. Because of the lower value of oxygen partial pressure in the inert flushing gas, the entropy of the product gases increases and hence thermal reduction is possible at lower temperatures.

The variation in the Gibbs free energy associated with the water splitting reaction (Figure 4) indicates that H_2 generation via water splitting using Sm produced after the reduction of Sm_2O_3 is possible below 6800 K (for a pressure of 1 bar). For a decrease in T_L from 6800 to 1900 K, ΔG_{ws} reduces by 1010 kJ·mol^{-1}. However, further lowering of T_L from 1900 to 300 K does not affect ΔG_{ws} significantly.

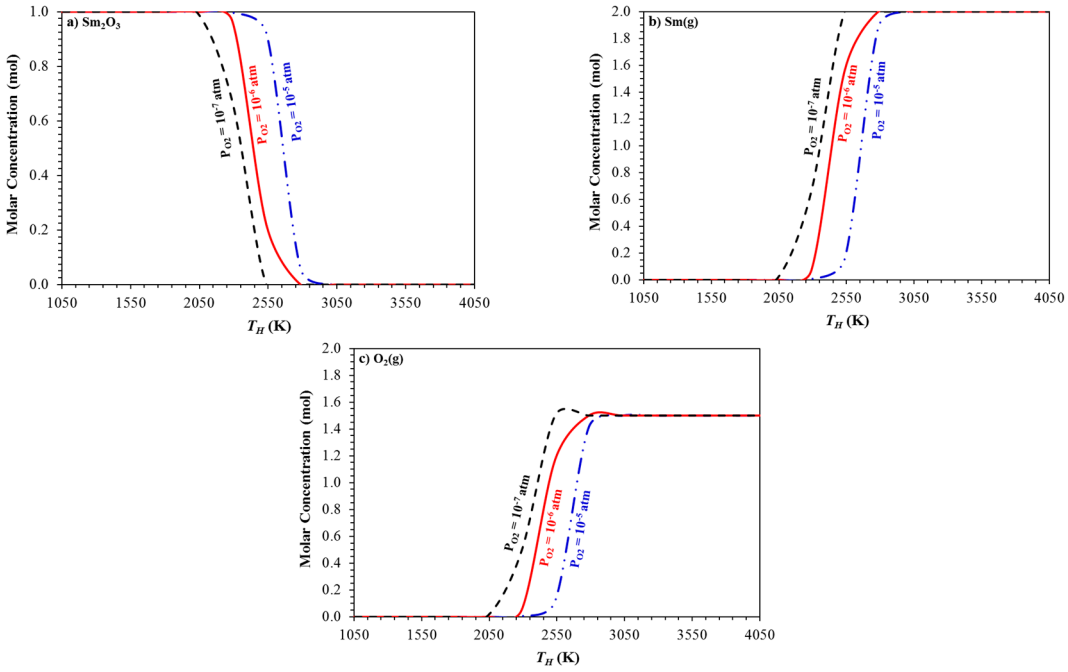

Figure 3. Effect of oxygen partial pressure in the inert flushing gas on equilibrium compositions related to the thermal reduction of Sm_2O_3. Change in the molar concentration of (**a**): Sm_2O_3; (**b**): Sm(g); (**c**): O_2(g).

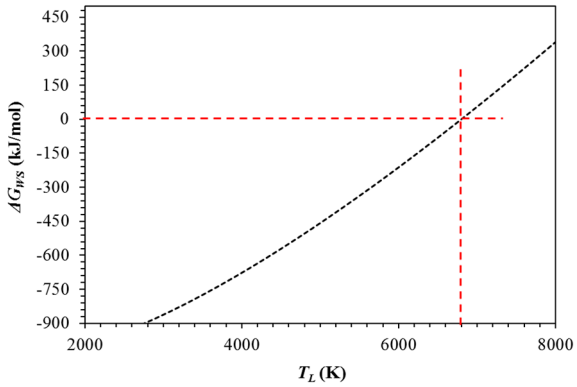

Figure 4. Variation in ΔG_{ws} as a function of T_L during H_2 production step.

3. Energy and Exergy Analyses

An exergy analysis of the Sm-WS cycle is carried out to provide a second law perspective. The process flow diagram for the Sm-WS cycle is shown in Figure 5. This cycle is comprised of a solar reactor, a quench unit, water splitting reactor, and a theoretical H_2/O_2 fuel cell. To perform the exergy analysis, the following assumptions are made:

- The production of H_2 is carried out at 1 bar and steady state conditions, with negligible viscous losses and changes in kinetic and potential energies.
- The solar reactor is considered a perfectly insulated blackbody absorber.
- The effective emissivity and absorptivity is both equal to unity.
- There are negligible convective/conductive heat losses.
- All reactions reach 100% completion.
- All products separate naturally without expending any work.
- Heat exchangers required for recovering the sensible and latent heat are omitted.

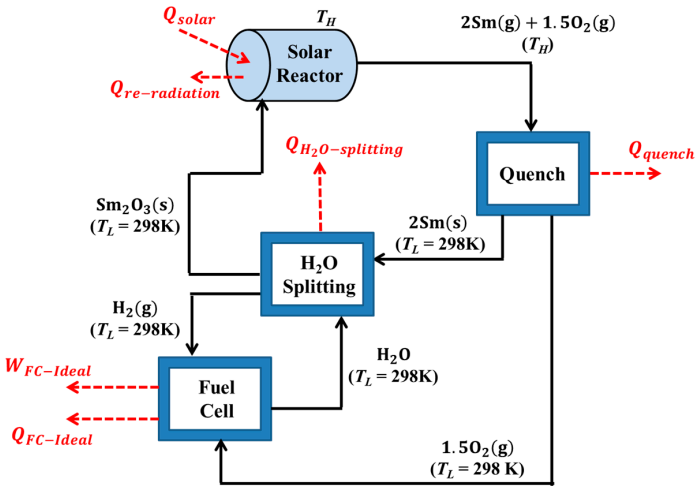

Figure 5. Process configuration for H_2 production via Sm-WS cycle.

The exergy analysis is performed following the methodology and governing equations derived and used previously for other MO based solar thermochemical cycles [6,9,10]. Thermodynamic properties are extracted from HSC software and databases and the analysis is normalized to a unit Sm_2O_3 molar flow rate (1 mol·s^{-1}) entering the solar reactor.

As a first step in the exergy analysis, the absorption efficiency ($\eta_{absorption}$), which is defined as the net rate at which energy is absorbed by the solar reactor divided by the solar energy input through the aperture, is determined as follows:

$$\eta_{absorption} = 1 - \left(\frac{\sigma T_H^4}{IC} \right) \quad (5)$$

Here, I denotes the direct normal solar irradiance *i.e.*, normal beam insolation (W/m), C denotes the solar flux concentration ratio (suns), T_H denotes the solar reactor temperature required for the thermal reduction of Sm_2O_3 and σ denotes the Stefan-Boltzmann constant (5.6705×10^{-8} W$\cdot$m$^{-2}\cdot$K^{-4}).

Values for $\eta_{absorption}$ calculated as a function of T_H are presented in Figure 6a. The trends indicate that $\eta_{absorption}$ increases with decreasing T_H. For instance, at T_H = 3000 K (oxygen partial pressure in the inert flushing gas = 10^{-5} bar), $\eta_{absorption}$ is 54%. As oxygen partial pressure in the inert flushing gas is further reduced to 10^{-8} bar, the corresponding T_H decreases by 720 K and $\eta_{absorption}$ rises to 84.7%.

The influence of C on $\eta_{absorption}$ (at constant T_H = 2280 K and oxygen partial pressure = 10^{-8} bar in the inert flushing gas) is also examined. At C = 2000 suns, $\eta_{absorption}$ is 23.4%. The efficiency $\eta_{absorption}$ can be increased to 38.3, 51.1, 57.5, and 61.3% by raising C to 4000, 6000, 8000, and 10,000 suns, respectively (Figure 6b).

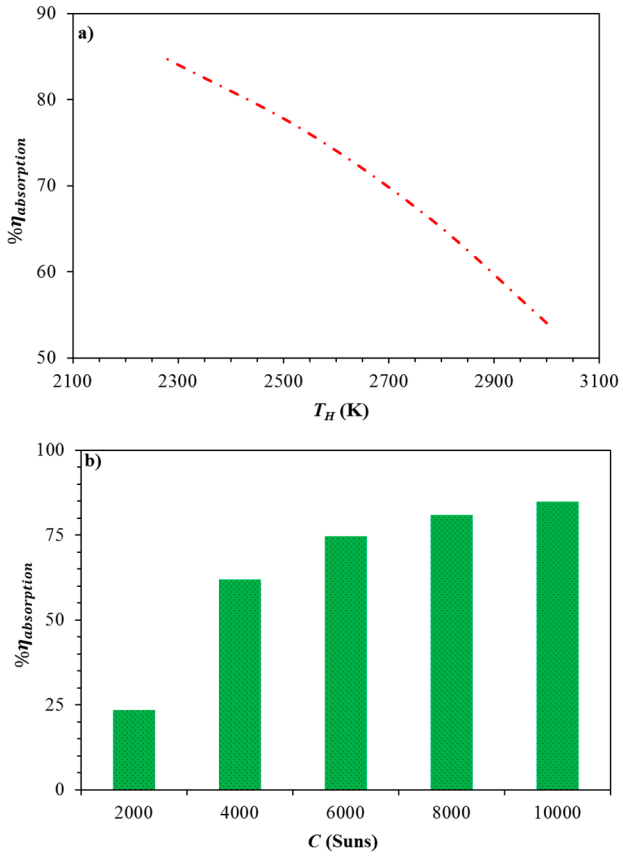

Figure 6. Effect of (**a**) T_H at C = 10,000 suns; and (**b**) C on $\eta_{absorption}$ at T_H = 2280 K.

To operate the Sm-WS cycle, solar energy is required 1) to heat the Sm_2O_3 from T_L to T_H and 2) for complete thermal reduction of Sm_2O_3 as per Equation (3). For comparison purposes, the heating of

Ar is not included in this calculation as it was not considered in previous studies. The net solar energy absorbed by the solar reactor to perform the above mentioned tasks can be calculated as:

$$Q_{reactor-net} = Q_{Sm_2O_3-heating} + Q_{Sm_2O_3-reduction} \quad (6)$$

$$Q_{Sm_2O_3-heating} = \dot{n}\Delta\ H|_{Sm_2O_3@T_L \rightarrow Sm_2O_3@T_H} \quad (7)$$

$$Q_{Sm_2O_3-reduction} = \dot{n}\Delta\ H|_{Sm_2O_3@T_H \rightarrow 2Sm(g)+1.5O_2(g)@T_H} \quad (8)$$

As per Figure 7, at T_H = 3000 K (when oxygen partial pressure = 10^{-5} bar in the inert flushing gas), $Q_{reactor-net}$ is 2583 kW. With a further decrease in oxygen partial pressure in the inert flushing gas, T_H reduces and the corresponding $Q_{reactor-net}$ values also decline. The value of $Q_{reactor-net}$ decreases by 82.3 and 120 kW with a decline in T_H to 2540 and 2280 K respectively as the oxygen partial pressure in the inert flushing gas is lowered to 10^{-7} and 10^{-8} bar.

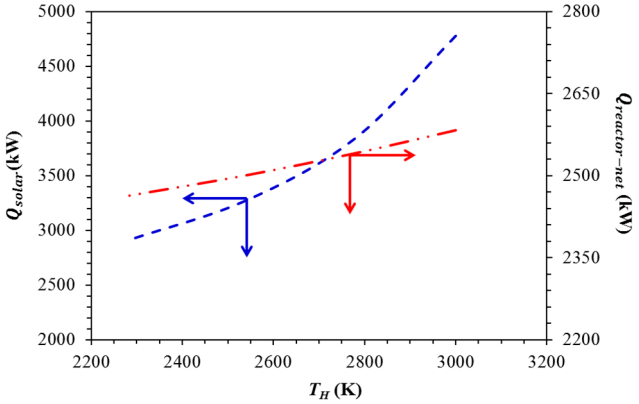

Figure 7. Effect of T_H on Q_{solar} and $Q_{reactor-net}$.

Based on the calculated values for $\eta_{absorption}$ and $Q_{reactor-net}$, the solar energy input required for the operation of Sm-WS cycle can be calculated as follows:

$$Q_{solar} = \frac{Q_{reactor-net}}{\eta_{absorption}} \quad (9)$$

The variation in Q_{solar} as a function of T_H is shown in Figure 7. It is seen that the maximum value of Q_{solar} (4777 kW) is needed at T_H = 3000 K (oxygen partial pressure in the inert flushing gas = 10^{-5} bar). Furthermore, the required value of Q_{solar} decreases as T_H reduces. For instance, at T_H = 2780 K (oxygen partial pressure = 10^{-6} bar in the inert flushing gas), Q_{solar} is 3248 kW. An additional drop in T_H to 2540 K (oxygen partial pressure = 10^{-7} bar in the inert flushing gas) reduces Q_{solar} to 3273 kW. The reason behind this lowering of Q_{solar} is the increase in $\eta_{absorption}$ due to the decline in T_H. Overall, as the oxygen partial pressure in the inert flushing gas decreases from 10^{-5} to 10^{-8} bar, T_H declines by 720 K and Q_{solar} by 39.1%.

Due to operation at elevated temperatures, radiation heat losses from the solar reactor are inevitable. The radiation heat losses associated with the solar reactor installed for the Sm-WS cycle can be calculated as:

$$Q_{re-radiation} = Q_{solar} - Q_{reactor-net} \quad (10)$$

The values of $Q_{re-radiation}$ reported in Table 1 indicate that radiation heat losses are greatest (2194 kW) when T_H = 3000 K (oxygen partial pressure in the inert flushing gas = 10^{-5} bar). A decrease in T_H results in a significant reduction in $Q_{re-radiation}$. This is again due to the fact that $\eta_{absorption}$ is higher at lower values of T_H. The quantity $Q_{re-radiation}$ can be lowered by 1748 kW with a decrease in

T_H to 2280 K (oxygen partial pressure = 10^{-8} bar in the inert flushing gas), which is a very significant reduction in input heat.

Table 1. Variation in Q_{quench} and $Q_{re-radiation}$ as a function of T_H.

T_H (K)	Q_{quench} (kW)	$Q_{re-radiation}$ (kW)
3000	756	2194
2780	714	1301
2540	673	773
2280	636	446

Products of the thermal reduction of Sm_2O_3 (*i.e.*, Sm and O_2) leaving the solar reactor are in the gas phase and also at high T_H. At such T_H levels, these gaseous products have a tendency to recombine and convert to Sm_2O_3. To avoid the re-formation of Sm_2O_3, the gaseous products exiting the solar reactor at T_H are rapidly cooled to T_L using a quench unit. During quenching, it is assumed that the chemical compositions of the products remain unaltered. The latent and sensible heat rejected by the quench unit can be determined as follows:

$$Q_{quench} = -\dot{n}\ \Delta H|_{2Sm(g)+1.5O_2(g)@T_H \rightarrow 2Sm(s)+1.5O_2(g)@T_L} \quad (11)$$

The thermal energy required for the separation of O_2 and the inert Ar (gas separation) is not considered for comparison purposes, as it was excluded in previous studies.

Table 1 reports the change in Q_{quench} with respect to T_H. It can be seen that, at higher T_H, Q_{quench} is also elevated. For instance, at T_H = 3000 K (oxygen partial pressure in the inert flushing gas = 10^{-5} bar), Q_{quench} is 756 kW. The data also confirm that the heat loss due to quenching can be reduced if the solar reactor is operated at a lower oxygen partial pressure in the inert flushing gas, which also results in a lower T_H. For instance, at an oxygen partial pressure in the inert flushing gas of 10^{-8} bar, the required values are T_H = 2280 K and Q_{quench} = 636 kW.

Irreversibilities associated with the solar reactor and quench unit due to the non-reversible chemical transformations and re-radiation losses to the surroundings can be calculated as:

$$Irr_{reactor} = \left(\frac{-Q_{solar}}{T_H}\right) + \left(\frac{Q_{re-radiation}}{298}\right) + \dot{n}\ \Delta S|_{Sm_2O_3@T_L \rightarrow 2Sm(g)+1.5O_2(g)@T_H} \quad (12)$$

$$Irr_{quench} = \left(\frac{Q_{quench}}{298}\right) + \dot{n}\ \Delta S|_{2Sm(g)+1.5O_2(g)@T_H \rightarrow 2Sm(s)+1.5O_2(g)@T_L} \quad (13)$$

Similarly, Q_{solar} and $Q_{reactor-net}$, as well as $Irr_{reactor}$ and Irr_{quench}, are also observed to be greatest at T_H = 3000 K (oxygen partial pressure in the inert flushing gas = 10^{-5} bar). As shown in Figure 8, the HSC simulation results indicate an 85.1% decrease in $Irr_{reactor}$ for a reduction in T_H from 3000 to 2280 K as the oxygen partial pressure in the inert flushing gas decreases to 10^{-8} bar. Correspondingly, Irr_{quench} is also lowered by 0.5 kW$\cdot$ K^{-1} due to a similar decline in T_H. These trends are in good agreement with the results reported in previous studies [9,10].

Solid Sm obtained after the quench unit (at 298 K) is transferred to the water splitting reactor (Sm oxidizer) and reacted with water at T_L = 298 K producing solar H_2. The rate of heat rejected to the surroundings by the water splitting reactor is estimated as 970 kW using the following equation and assuming 100% conversion:

$$Q_{Sm\ oxidation} = -\dot{n}\ \Delta H|_{2Sm+3H_2O \rightarrow Sm_2O_3+\ 3H_2(g)@T_L} \quad (14)$$

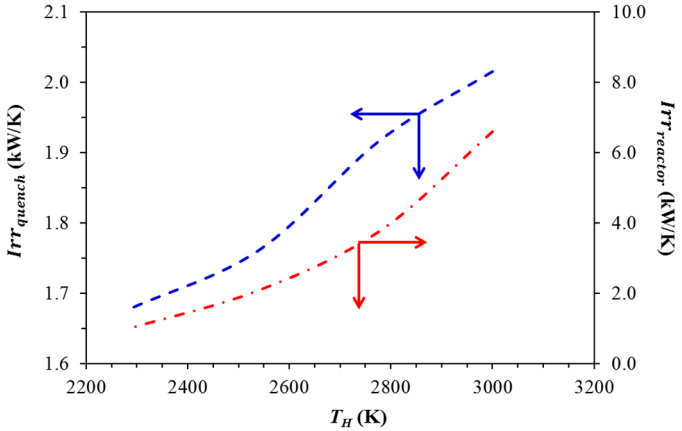

Figure 8. Effect of T_H on $Irr_{reactor}$ and Irr_{quench}.

Also, the irreversibility associated with the water splitting reactor is observed to be 3.5 kW· K^{-1} using the following equation:

$$Irr_{Sm\ oxidation} = \left(\frac{Q_{Sm\ oxidation}}{298}\right) + \dot{n}\ \Delta S|_{2Sm+3H_2O \rightarrow Sm_2O_3 + 3H_2(g)@T_L} \quad (15)$$

An ideal H_2/O_2 fuel cell is added to the Sm-WS cycle to extract the maximum work from the net H_2 produced. In this study, the efficiency of the H_2/O_2 fuel cell is considered as 100% and hence it is defined as an ideal fuel cell. The following two equations can be used to determine the theoretical rate of work performed (711 kW) and heat energy released (146 kW) by the H_2/O_2 fuel cell:

$$W_{FC-Ideal} = -\dot{n}\ \ \Delta G|_{3H_2(g)+1.5O_2(g) \rightarrow 3H_2O(l)@298K} \quad (16)$$

$$Q_{FC-Ideal} = -(298) \times \dot{n}\ \ \Delta S|_{3H_2(g)+1.5O_2(g) \rightarrow 3H_2O(l)@298K} \quad (17)$$

In the case of solar thermochemical cycles, the cycle efficiency (η_{cycle}) is defined as the ratio of theoretical work performed by the ideal fuel cell to the solar energy input:

$$\eta_{cycle} = \frac{W_{FC-Ideal}}{Q_{solar}} \quad (18)$$

Similarly, the solar-to-fuel-conversion efficiency ($\eta_{solar-to-fuel}$) can be defined as the ratio of higher heating value (*HHV*) of the H_2 produced to the solar energy input:

$$\eta_{solar-to-fuel} = \frac{HHV_{H_2}}{Q_{solar}} \quad (19)$$

Both η_{cycle} and $\eta_{solar-to-fuel}$ of the Sm-WS cycle are estimated based on the HSC simulation results and given in Table 2. The values for η_{cycle} and $\eta_{solar-to-fuel}$ increase as T_H decreases. At T_H = 3000 K (oxygen partial pressure in the inert flushing gas = 10^{-5} bar), η_{cycle} is 14.9% and $\eta_{solar-to-fuel}$ is 17.9%. For a reduction in T_H to 2280 K due to the decline in oxygen partial pressure in the inert flushing gas to 10^{-8} bar, both η_{cycle} and $\eta_{solar-to-fuel}$ can be increased up to 24.5% and 29.5%, respectively. These efficiency values are comparable with other MO cycles such as the ZnO/Zn cycle (29%) [5], the SnO_2/SnO cycle (29.8%) [33], the Fe_3O_4/FeO cycle (30%) [34] and the ceria cycle (20.2%) [29], which all were investigated previously employing similar operating conditions.

Table 2. Values for η_{cycle} and $\eta_{solar-to-fuel}$ as a function of T_H.

T_H (K)	η_{cycle} (%)	$\eta_{solar-to-fuel}$ (%)
3000	14.9	17.9
2780	18.5	22.3
2540	21.7	26.2
2280	24.5	29.5

By applying heat recuperation, η_{cycle} and $\eta_{solar-to-fuel}$ for the Sm-WS cycle can be further enhanced [19,29,35]. Heat rejected by the quench unit and the water splitting reactor can be recycled and re-utilized to drive the Sm-WS cycle. The total amount of heat that can be recuperated is calculated as:

$$Q_{recuperable} = Q_{quench} + Q_{Sm\ oxidation} \tag{20}$$

With the inclusion of the heat recuperation, the solar energy required for the operation of the cycle can be reduced as follows:

$$Q_{solar,\ with\ recuperation} = Q_{solar} - \left[(\%\ recuperation) \times Q_{recuperable}\right] \tag{21}$$

As an example, the alteration in $Q_{solar,\ with\ recuperation}$ and $Q_{recuperable}$ as a function of % heat recuperation for the case of T_H = 2280 K (oxygen partial pressure in the inert flushing gas = 10^{-8} bar) is shown in Figure 9. The results indicate that, as the % heat recuperation increases, $Q_{recuperable}$ rises whereas $Q_{solar,\ with\ recuperation}$ declines. For instance, with no heat recuperation, $Q_{solar,\ with\ recuperation}$ = 2909 kW. But as heat recuperation increases to 50%, $Q_{solar,\ with\ recuperation}$ decreases to 2106 kW, with 803 kW of the thermal energy recycled from the quench unit and water splitting reactor to drive the Sm-WS cycle.

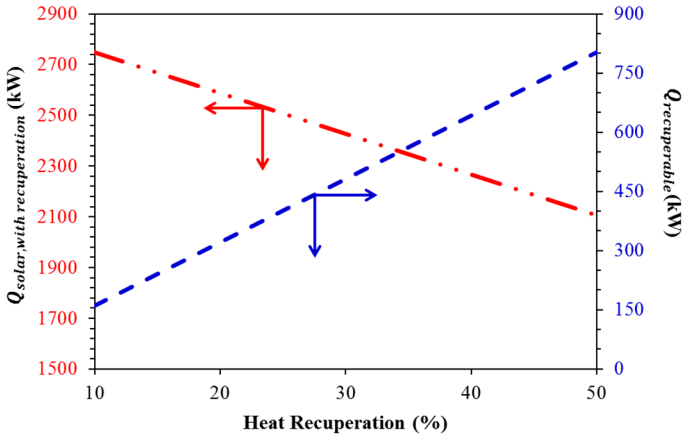

Figure 9. Effect of % heat recuperation on $Q_{solar,\ with\ recuperation}$ and $Q_{recuperable}$ (T_H = 2280 K).

The efficiencies η_{cycle} and $\eta_{solar-to-fuel}$ after heat recuperation can be determined as:

$$\eta_{cycle} = \frac{W_{FC-Ideal}}{Q_{solar,with\ recuperation}} \tag{22}$$

$$\eta_{solar-to-fuel} = \frac{HHV_{H_2}}{Q_{solar,with\ recuperation}} \tag{23}$$

The effects of heat recuperation on η_{cycle} and $\eta_{solar-to-fuel}$ for all T_H values are provided in Table 3. Also, the increase in η_{cycle} and $\eta_{solar-to-fuel}$ due to heat recuperation for the case of T_H = 2280 K

(oxygen partial pressure in the inert flushing gas = 10^{-8} bar) is presented in Figure 10. The data reported in Table 3 and Figure 10 confirm that, as heat recuperation is employed, both η_{cycle} and $\eta_{solar-to-fuel}$ increase significantly. For example, at T_H = 2280 K, η_{cycle} and $\eta_{solar-to-fuel}$ (without heat recuperation) are 24.5% and 29.5%. However, if 60% heat recuperation is employed, both η_{cycle} and $\eta_{solar-to-fuel}$ can be raised further, to 36.5% and 44.1%, respectively. These efficiency values are much higher than for previously examined MO cycles (Table 4).

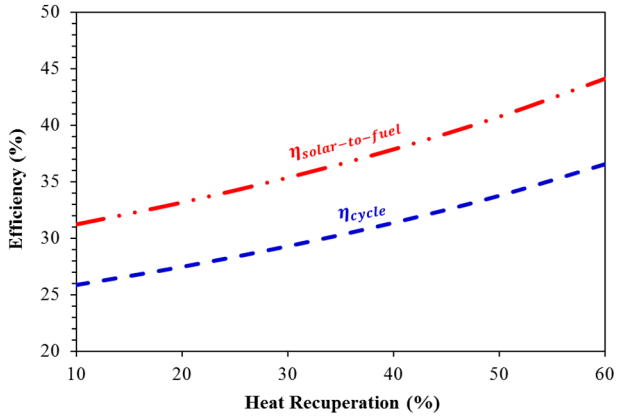

Figure 10. Effect of % heat recuperation on η_{cycle} and $\eta_{solar-to-fuel}$ (T_H = 2280 K).

Table 3. η_{cycle} and $\eta_{solar-to-fuel}$ for Sm-WS cycle.

T_H (K)	η_{cycle} (%)	$\eta_{solar-to-fuel}$ (%)
Recuperation = 0%		
2780	18.5	22.3
2540	21.7	26.2
2280	24.4	29.5
Recuperation = 20%		
2780	20.3	24.5
2540	24.1	29.1
2280	27.5	33.1
Recuperation = 40%		
2780	22.4	27.1
2540	27.2	32.8
2280	31.4	37.8
Recuperation = 60%		
2780	25.1	30.3
2540	31.1	37.5
2280	36.5	44.1

Table 4. Comparison between Sm-WS cycle and previously investigated metal oxide based cycles in terms of $\eta_{solar-to-fuel}$.

Cycle	$\eta_{solar-to-fuel}$ (%)
Zinc oxide cycle	29.0
Tin oxide cycle	29.8
Iron oxide cycle	30.0
Ceria cycle	20.2
Sm-WS cycle	44.1

The exergy analysis performed for the Sm-WS cycle can be verified by conducting an energy balance and evaluating the maximum achievable efficiency from the total available work and from the total solar power input. The energy balance (for all T_H) confirms that:

$$W_{FC-Ideal} = Q_{solar} - \left(Q_{re-radiation} + Q_{quench} + Q_{Sm\ oxidation} + Q_{FC-Ideal}\right) \quad (24)$$

At T_H = 2540 K, the energy balance in Equation (24) indicates that $W_{FC-Ideal}$ = 712 kW which is equal to $W_{FC-Ideal}$ determined by Equation (16). Likewise, at T_H = 2280 K, the energy balance indicates that $W_{FC-Ideal}$ = 712 kW which is again equal to the value of $W_{FC-Ideal}$ determined by Equation (16). The available work can be estimated as the addition of the work done by the fuel cell and the work lost due to the irreversibilities in the solar reactor, quench unit, and water splitting reactor. In case of the Sm-WS cycle, the maximum cycle efficiency can be calculated as:

$$\eta_{cycle,maximum} = \frac{W_{FC-Ideal} + T_L\left(Irr_{reactor} + Irr_{quench} + Irr_{sm\ oxidation}\right)}{Q_{solar}} \quad (25)$$

For all values of T_H, it is observed that $\eta_{cycle,maximum}$ is equal to the efficiency of a Carnot heat engine operating between hot and cold temperature reservoirs:

$$\eta_{cycle,maximum} = 1 - \frac{T_L}{T_H} = \eta_{carnot} \quad (26)$$

For instance, at T_H = 2280 K and T_L = 298 K, $\eta_{cycle,maximum}$ = 86.9% which is equal to η_{carnot} = 86.9%. Similarly, at T_H = 2780 K and T_L = 298 K, $\eta_{cycle,maximum}$ = 89.3% which is again equal to η_{carnot} = 89.3%.

From the results obtained during this investigation (phase–1: thermodynamic analysis), we have realized that the temperatures required in case of Sm-WS cycle are significantly higher. To overcome this limitation, we are currently working towards improving the redox reactivity of Sm_2O_3 at lower temperatures by synthesizing doped Sm_2O_3. The host, *i.e.*, Sm_2O_3, will be doped by suitable metal cations such as Ni, Mn, Co, Fe, Ce, and others using various synthesis approaches such as sol-gel, co-precipitation, combustion synthesis, *etc.* It is expected that in the case of doped Sm_2O_3, the temperatures required for thermal reduction will be lower as compared to pure Sm_2O_3. This second phase of this investigation is underway in our laboratories.

4. Conclusions

The thermodynamic feasibility of a Sm-WS cycle for the production of solar hydrogen is investigated. HSC simulation results indicate that the temperature (T_H) required for complete thermal reduction of Sm_2O_3 can be significantly decreased with a reduction in the oxygen partial pressure in the inert flushing gas used inside the reactor. For instance, at oxygen partial pressure in the inert flushing gas = 10^{-5} bar, T_H is 3000 K. As the oxygen partial pressure in the inert flushing gas decreases to 10^{-8} bar, T_H can be lowered to 2280 K. Thermodynamic calculations confirm that the water splitting reaction via Sm oxidation is feasible below 6800 K.

The exergy analysis of the Sm-WS cycle indicates that $\eta_{absorption}$ can be increased by 30.61% due to the decrease in T_H from 3000 to 2280 K as the oxygen partial pressure in the inert flushing gas reduces from 10^{-5} to 10^{-8} bar. In contrast, $\eta_{absorption}$ can be reduced by 61.3% with a decrease in the value of C from 10,000 to 2000 suns (at T_H = 2280 K). The quantities $Q_{reactor-net}$ and Q_{solar} can also be lowered by 4.6 and 39.1% as T_H falls from 3000 to 2280 K. Correspondingly, the heat losses due to quenching and re-radiation can be reduced by 120 and 1748 kW for a similar reduction in T_H. The lower solar energy input requirements and heat losses during quenching and re-radiation are possible as $\eta_{absorption}$ increases with decreasing T_H. The maximum efficiencies, η_{cycle} = 24.5% and $\eta_{solar-to-fuel}$ = 29.5%, are observed at lower values of T_H = 2280 K and oxygen partial pressure in the inert flushing gas = 10^{-8} bar (with no heat recuperation). These efficiency values can be further

enhanced by recycling the heat recuperated from the quench unit and water splitting reactor to drive the cycle. For instance, at heat recuperation levels of 20%, 40% and 60%, $\eta_{solar-to-fuel}$ can be increased by a factor of 1.12, 1.28, and 1.49, respectively.

Acknowledgments: This publication was made possible by the NPRP grant (NPRP8-370-2-154) and UREP grant (UREP18-146-2-060) from the Qatar National Research Fund (a member of Qatar Foundation). The statements made herein are solely the responsibility of author(s). The authors also gratefully acknowledge the financial support provided by the Qatar University Internal Grant (QUUG-CENG-CHE-14\15-10).

Author Contributions: This investigation is mainly performed at Qatar University under the guidance of Rahul Bhosale. Other co-authors have contributed in terms of their technical inputs towards the thermodynamic calculations, analysis of the data, and final manuscript preparation.

Conflicts of Interest: The authors declare no conflict of interest.

Nomenclature

C	Solar flux concentration ratio (suns)
I	Normal beam solar insolation ($W \cdot m^{-2}$)
$\dot{n}$	Molar flow rate ($mol \cdot s^{-1}$)
Q_{quench}	Heat rejection rate to surroundings from quench unit (kW)
$Q_{FC-Ideal}$	Heat rejection rate to surroundings from ideal fuel cell (kW)
$Q_{Sm\ oxidation}$	Heat rejection rate to surroundings from water splitting reactor (kW)
$Q_{Sm_2O_3-heating}$	Energy rate required for heating of Sm_2O_3 (kW)
$Q_{Sm_2O_3-reduction}$	Energy rate required for the thermal reduction of Sm_2O_3 (kW)
$Q_{reactor-net}$	Net energy input rate required for the operation of Sm-WS cycle (kW)
$Q_{re-radiation}$	Radiation heat loss rate from the solar reactor (kW)
$Q_{recuperable}$	Total heat rate that can be recuperated (kW)
Q_{solar}	Solar energy input rate (kW)
$Q_{solar,with\ recuperation}$	Solar power input after heat recuperation (kW)
T_H	Thermal reduction temperature (K)
T_L	Water splitting temperature (K)
$W_{FC-Ideal}$	Work rate output of ideal fuel cell (kW)
$\eta_{absorption}$	Solar absorption efficiency
η_{cycle}	Cycle efficiency
$\eta_{solar-to-fuel}$	Solar to fuel energy conversion efficiency
ΔG_{WS}	Gibbs free energy change for water splitting reaction ($kJ \cdot mol^{-1}$)
σ	Stefan–Boltzmann constant, 5.670×10^{-8} ($W \cdot m^{-2} \cdot K^{-4}$)
$Irr_{reactor}$	Rate of entropy produced across solar reactor ($kW \cdot K^{-1}$)
Irr_{quench}	Rate of entropy produced across quench unit ($kW \cdot K^{-1}$)
$Irr_{Sm\ oxidation}$	Rate of entropy produced across water splitting reactor ($kW \cdot K^{-1}$)

References

1. International Energy Agency. *CO_2 Emissions from Fuel Combustion*, 2015th ed.; International Energy Agency: Paris, France, 2015.
2. Scheffe, J.R.; Steinfeld, A. Oxygen exchange materials for solar thermochemical splitting of H_2O and CO_2: A review. *Mater. Today* **2014**, *17*, 341–348. [CrossRef]
3. Roeb, M.; Neises, M.; Monnerie, N.; Call, F.; Simon, H.; Sattler, C.; Schmucker, M.; Pitz-Pall, R. Materials-related aspects of thermochemical water and carbon dioxide splitting: A review. *Materials* **2012**, *5*, 2015–2054. [CrossRef]
4. Smestad, G.P.; Steinfeld, A. Review: Photochemical and thermochemical production of solar fuels from H_2O and CO_2 using metal oxide catalysts. *Ind. Eng. Chem. Res.* **2012**, *51*, 11828–11849. [CrossRef]
5. Steinfeld, A. Solar hydrogen production via a two-step water-splitting thermochemical cycle based on Zn/ZnO redox reactions. *Int. J. Hydrog. Energy* **2002**, *27*, 611–619. [CrossRef]
6. Steinfeld, A. Solar thermochemical production of hydrogen–A review. *Sol. Energy* **2005**, *78*, 603–615. [CrossRef]

7. Abanades, S.; Charvin, P.; Flamant, G. Design and simulation of a solar chemical reactor for the thermal reduction of metal oxides: Case study of zinc oxide dissociation. *Chem. Eng. Sci.* **2007**, *62*, 6323–6333. [CrossRef]
8. Galvez, M.E.; Loutzenhiser, P.G.; Hischier, I.; Steinfeld, A. CO_2 splitting via two-step solar thermochemical cycles with Zn/ZnO and FeO/Fe_3O_4 redox reactions II: Kinetic analysis. *Energy Fuels* **2009**, *23*, 2832–2839.
9. Loutzenhiser, P.G.; Steinfeld, A. Solar syngas production from CO_2 and H_2O in a two-step thermochemical cycle via Zn/ZnO redox reactions: Thermodynamic cycle analysis. *Int. J. Hydrog. Energy* **2011**, *36*, 12141–12147. [CrossRef]
10. Loutzenhiser, P.G.; Meier, A.; Steinfeld, A. Review of the two-step H_2O/CO_2-splitting solar thermochemical cycle based on Zn/ZnO redox reactions. *Materials* **2010**, *3*, 4922–4938. [CrossRef]
11. Dardor, D.; Bhosale, R.R.; Gharbia, S.; Kumar, A.; AlMomani, F. Solar carbon production via thermochemical ZnO/Zn carbon dioxide splitting cycle. *J. Emerg. Trends Eng. Appl. Sci.* **2015**, *6*, 129–135.
12. Miller, J.E.; Allendorf, M.D.; Diver, R.B.; Evans, L.R.; Siegel, N.P.; Stuecker, J.N. Metal oxide composites and structures for ultra-high temperature solar thermochemical cycles. *J. Mater. Sci.* **2008**, *43*, 4714–4728. [CrossRef]
13. Ishihara, H.; Kaneko, H.; Hasegawa, N.; Tamaura, Y. Two-step water-splitting at 1273–1623K using yttria-stabilized zirconia-iron oxide solid solution via co-precipitation and solid-state reaction. *Energy* **2008**, *33*, 1788–1793. [CrossRef]
14. Bhosale, R.R.; Kumar, A.; van den Broeke, L.J.P.; Gharbia, S.; Dardor, D.; Jilani, M.; Folady, J.; Al-Fakih, M.S.; Tarsad, M.A. Solar hydrogen production via thermochemical iron oxide–iron sulfate water splitting cycle. *Int. J. Hydrog. Energy* **2015**, *40*, 1639–1650. [CrossRef]
15. Bhosale, R.R.; Kumar, A.; AlMomani, F.A.; Alxneit, I. Sol–gel derived CeO_2–Fe_2O_3 nanoparticles: Synthesis, characterization and solar thermochemical application. *Ceram. Int.* **2016**. in press. [CrossRef]
16. Abanades, S. CO_2 and H_2O reduction by solar thermochemical looping using SnO_2/SnO redox reactions: Thermogravimetric analysis. *Int. J. Hydrog. Energy* **2012**, *37*, 8223–8231. [CrossRef]
17. Charvin, P.; Abanades, S.; Lemont, F.; Flamant, G. Experimental study of SnO_2/SnO/Sn thermochemical systems for solar production of hydrogen. *AIChE J.* **2008**, *54*, 2759–2767. [CrossRef]
18. Dardor, D.; Bhosale, R.R.; Gharbia, S.; AlNouss, A.; Kumar, A.; AlMomani, F. Solar thermochemical conversion of CO_2 into C via SnO_2/SnO redox cycle: Thermodynamic study. *Int. J. Eng. Res. Appl.* **2015**, *5*, 134–140.
19. Bhosale, R.R.; Kumar, A.; Almomani, F. Solar thermochemical hydrogen production via terbium oxide based redox reactions. *Int. J. Photoenergy* **2016**, *2016*. [CrossRef]
20. Agrafiotis, C.C.; Pagkoura, C.; Zygogianni, A.; Karagiannakis, G.; Kostoglou, M.; Konstandopoulos, A.G. Hydrogen production via solar-aided water splitting thermochemical cycles: Combustion synthesis and preliminary evaluation of spinel redox-pair materials. *Int. J. Hydrog. Energy* **2012**, *37*, 8964–8980. [CrossRef]
21. Bhosale, R.R.; Khadka, R.; Puszynski, J.; Shende, R. H_2 generation from two-step thermochemical water-splitting reaction using sol-gel derived $Sn_xFe_yO_z$. *J. Renew. Sustain. Energy* **2011**, *3*, 063104. [CrossRef]
22. Scheffe, J.; Li, J.; Weimer, A. A spinel ferrite/hercynite water-splitting redox cycle. *Int. J. Hydrog. Energy* **2010**, *35*, 3333–3340. [CrossRef]
23. Bhosale, R.R.; Shende, R.V.; Puszynski, J.A. Thermochemical water-splitting for H_2 generation using sol-gel derived Mn-ferrite in a packed bed reactor. *Int. J. Hydrog. Energy* **2012**, *37*, 2924–2934. [CrossRef]
24. Bhosale, R.R.; Kumar, A.; AlMomani, F.A.; Alxneit, I. Propylene oxide assisted sol-gel synthesis of zinc ferrite nanoparticles for solar fuel production. *Ceram. Int.* **2016**, *42*, 2431–2438. [CrossRef]
25. Roeb, M.; Gathmann, N.; Neises, M.; Sattler, C.; Pitz-Paal, R. Thermodynamic analysis of two-step solar water splitting with mixed iron oxides. *Int. J. Energy Res.* **2009**, *33*, 893–902. [CrossRef]
26. Bader, R.; Venstrom, L.J.; Davidson, J.H.; Lipiński, W. Thermodynamic analysis of isothermal redox cycling of ceria for solar fuel production. *Energy Fuels* **2013**, *27*, 5533–5544. [CrossRef]
27. Chueh, W.C.; Falter, C.; Abbott, M.; Scipio, D.; Furler, P.; Haile, S.M.; Steinfeld, A. High-flux solar-driven thermochemical dissociation of CO_2 and H_2O using nonstoichiometric ceria. *Science* **2010**, *330*, 1797–1801. [CrossRef] [PubMed]
28. Furler, P.; Scheffe, J.R.; Steinfeld, A. Syngas production by simultaneous splitting of H_2O and CO_2 via ceria redox reactions in a high-temperature solar reactor. *Energy Environ. Sci.* **2012**, *5*, 6098–6103. [CrossRef]

29. Scheffe, J.R.; Steinfeld, A. Thermodynamic analysis of cerium-based oxides for solar thermochemical fuel production. *Energy Fuels* **2012**, *26*, 1928–1936. [CrossRef]
30. Scheffe, J.R.; Weibel, D.; Steinfeld, A. Lanthanum–strontium–manganese perovskites as redox materials for solar thermochemical splitting of H_2O and CO_2. *Energy Fuels* **2013**, *27*, 4250–4257. [CrossRef]
31. Demont, A.; Abanades, S. High redox activity of Sr-substituted lanthanum manganite perovskites for two-step thermochemical dissociation of CO_2. *RSC Adv.* **2014**, *4*, 54885–54891. [CrossRef]
32. Gálvez, M.; Jacot, R.; Scheffe, J.R.; Cooper, T.; Patzke, G.; Steinfeld, A. Physico-chemical changes in Ca, Sr and Al-doped La–Mn–O perovskites upon thermochemical splitting of CO_2 via redox cycling. *Phys. Chem. Chem. Phys.* **2015**, *17*, 6629–6634. [CrossRef] [PubMed]
33. Roine, A. *Outokumpu HSC Chemistry for windows, version 7.1.*; Outokumpu Research Oy: Pori, Finland, 2013.
34. Abanades, S.; Charvin, P.; Lemont, F.; Flamant, G. Novel two-step SnO_2/SnO water-splitting cycle for solar thermochemical production of hydrogen. *Int. J. Hydrog. Energy* **2008**, *33*, 6021–6030. [CrossRef]
35. Diver, R.B.; Miller, J.E.; Allendorf, M.D.; Seigel, N.P.; Hogan, R.E. Solar thermochemical water-splitting ferrite-cycle heat engines. *J. Sol. Energy Eng.* **2008**, *130*, 041001. [CrossRef]